Experimental investigation of the self- and N_2-broadened continuum within the ν_2 band of water vapor

David C. Tobin, L. Larrabee Strow, Walter J. Lafferty, and W. Bruce Olson

We present an experimental study of the self- and N_2-broadened H_2O continuum in microwindows within the ν_2 fundamental centered at ~1600 cm^{-1}. The continuum is derived from transmission spectra recorded at room temperature with a BOMEM Fourier transform spectrometer at a resolution of ~0.040 cm^{-1}. Although we find general agreement with previous studies, our results suggest that there is significant near-wing super-Lorentzian behavior that produces a highly wave-number-dependent structure in the continuum as it is currently defined.

Key words: Infrared absorption, water vapor, continuum, spectral line shape, Fourier transform spectrometer.

1. Introduction

Deviations of H_2O spectral line shapes from Lorentz have been studied extensively for the atmospheric windows at 4 and 10 μm, and several thorough reviews exist.[1,2] Non-Lorentzian H_2O line shapes can also have a significant impact within the strong pure rotational and vibrational bands. This in-band continuum is particularly important for satellite infrared remote sensing of atmospheric H_2O profiles. For example, the Atmospheric Infrared Sounder[3,4] is an upcoming temperature and humidity sounder that has H_2O channels located continuously throughout the ν_2 P branch. An accurate retrieval of the H_2O profile from the channel radiances requires a detailed knowledge of atmospheric water vapor transmittances inside the band, especially between lines where the radiative transfer weighting functions vary most sharply with altitude.

For well-isolated pressure-broadened lines in the infrared, the Lorentzian line shape is very accurate near the line center. However, calculations based on the impact approximation generally overestimate the observed absorption in the far-wing window regions and underestimate the absorption within the rotational and vibrational bands. If all lines have the same line shape, these errors lead to the conclusions that the actual water vapor line shape is extremely sub-Lorentzian in the far wing and at least somewhat super-Lorentzian in the intermediate or near wing. Because most experimental studies have focused on the window regions, the far-wing line shape has received most of the attention and its behavior has been characterized more accurately than the near-wing line shape (roughly within 5–25 cm^{-1} of the line center).

A recent paper by Tipping and Ma[5] contains a useful summary of the history of theoretical research on water vapor line shapes and will not be repeated in detail here. Considerable progress in the past 15 years was initiated by Clough *et al.*[6] with the development of a rigorous foundation for an autocorrelation function approach that takes the finite duration of collisions into account. Using a single line shape for all lines and several adjustable parameters, they greatly improved the agreement between theory and experiment over impact theory and provided a realistic physical framework for accurate parameterizations.[7,8] Further developments of the fundamental theory by Rosenkranz[9,10] and by Tipping and Ma[5] use a statistical quasistatic approach and attempt to represent the line shape by using the intermolecular potentials with no adjustable parameters. Their extensive research can reproduce many of the existing

D. C. Tobin and L. Larrabee Strow are with the Department of Physics, University of Maryland Baltimore County, Baltimore, Maryland 21228. W. J. Lafferty is with the Molecular Physics Division, National Institute of Standards and Technology, Gaithersburg, Maryland 20899. W. B. Olson is at 348 North Summit Avenue, Gaithersburg, Maryland 20877.

Received 13 November 1995; revised manuscript received 11 March 1996.

0003-6935/96/244724-11$10.00/0

water continuum measurements to an accuracy that validates their approach in the far wings of the lines, but it may not be sufficiently accurate for some applications.[8]

All of these approaches have been oriented toward modeling far-wing non-Lorentzian behavior in order to predict radiative transfer in the atmospheric windows, and consequently they are least accurate in the near-wing of the line, which is also more difficult to handle theoretically. Clough's subsequent parameterizations[7,8] of his theoretical line shape bring it into better agreement with the experiment inside bands, where near-wing line shape effects are more important. These so-called CKD models (in which CKD stands for Clough, Kneizys, and Davies) are widely used in a variety of atmospheric applications. Ma and Tipping[11,12] are working to improve their calculations of the near-wing behavior but have them remain within the quasistatic framework. Despite these efforts, an accurate near-wing line shape does not exist, partially because of a lack of adequate laboratory data for the testing of theory. These considerations have prompted the measurements presented here.

The most notable experimental studies of the water vapor continuum within the ν_2 band are those of Burch and co-workers.[13–16] Their research was carried out a number of years ago at relatively low spectral resolution. The wave-number regions for these studies were chosen to be at the centers of the so-called microwindows such that the absorption caused by lines within $\sim 1\ cm^{-1}$ could be ignored and so that the low instrument resolution would not distort the spectra. Because of a lack of other laboratory measurements, these results have formed the benchmark for theoretical comparisons in this spectral region.

Thériault *et al.*[17] recently recorded atmospheric transmission spectra over a horizontal path of 5.7 km. These spectra were utilized to test the accuracy of the existing H_2O continuum. Their results suggest that, in the wings of the ν_2 band, the foreign component of the CKDv0 continuum must be decreased by approximately a factor of 2 to obtain good agreement with the experiment. Derivation of the H_2O continuum from atmospheric transmission spectra is a complex task that has its own specific limitations because of difficulties in characterizing the amount of water vapor and other interfering species in the optical path. Laboratory measurements offer better control of these parameters, but often with insufficient optical depth to study regions of weaker absorption. Consequently, our two transmission measurements are complementary—theirs are better in the weaker band wings, and ours are better within the band.

Atmospheric emission spectra from the University of Wisconsin High-Resolution Interferometer (HIS)[17–19] show that large errors remain in the water continuum. These spectra are very sensitive to the continuum and provide an excellent test of water continuum models when the atmospheric state is well characterized. Differences between observed and calculated high-resolution atmospheric radiances can be as large as 4 K in brightness temperature in between lines inside the ν_2 band when Clough's original water continuum model (CKDv0) is used.[17,20,21] Clough recently modified his continuum model (CKDv2.1) and obtained better agreement with several types of atmospheric observations.[8,17,19] In particular the atmospheric studies suggested that the nitrogen-broadened continuum near $\sim 1200\ cm^{-1}$ was approximately a factor of 2 smaller than predicted by CKDv0. This improved model (CKDv2.1) reduces the maximum errors in HIS calculated radiances to ~ 2 K in between spectral lines in the 1200 cm^{-1} region.[22] The remaining errors are highly dependent on wave number.

The best humidity sounding channels are located in between the ν_2 spectral lines, where the water transmittance errors remain much larger than desirable for satellite retrievals of the H_2O profile. The Atmospheric Infrared Sounder will have noise levels below 0.2 K in this region, far below the existing accuracy of the H_2O continuum.

We have recorded a large series of laboratory spectra of high-optical-depth H_2O to improve our knowledge of the ν_2 in-band H_2O continuum. Our first goal was to verify the accuracy of Burch's measurements in this region. We also wanted a more dense wave-number coverage of the continuum for satellite remote sensing applications. Our laboratory spectra will also provide a good test for new theoretical and model calculations, which have been limited by the sparsity of Burch's measurements. We were also prompted to do these measurements because the HIS observations indicated the need for wave-number-dependent changes to the continuum that are initially best studied with laboratory data.

We report here an analysis of our measurements of the self- and N_2-broadened H_2O continuum in the region 1350–2100 cm^{-1} recorded with a high-resolution Fourier transform spectrometer. A direct comparison with the research of Burch is made in that we generally report the continuum at the same wave numbers as Burch, as well as in other microwindows. The main difference between Burch's research and our research is that our measurements were made at relatively high spectral resolution, generally 0.04 cm^{-1}. Because the wave numbers chosen by Burch are in microwindows that are largely unaffected by his lower spectral resolution, we should be able to compare our results directly with his. Because existing H_2O continuum models are largely based on the research of Burch, we felt it was worthwhile to report our results initially in a form that is directly comparable with his research and that can be easily used by others for atmospheric calculations in these microwindows. The analysis of continuum measurements made at a much denser wave-number scale throughout the ν_2 band and the implications for atmospheric H_2O continuum models will be reported in an upcoming paper.

2. Experimental

The experimental data presented here were collected at the Molecular Physics Division of the National Institute of Standards and Technology (NIST) by using a BOMEM DA3.002 Fourier transform spectrometer coupled to a long-path White-type absorption cell.[23] Spectra were recorded between 1150 and 2250 cm^{-1} by using a Globar source, a KBr beam splitter, CaF_2 windows on the input and output ports of the absorption cell, and a narrow-range MgCdTe detector.

The cell and the transfer optics aligning it to the spectrometer are designed to minimize astigmatism.[24] The entire optical path from the source to the detector can be evacuated. The White-type cell is modified from White's original design and is described here briefly. The cell has a base path length of 2 m and possible optical path lengths of 4, 12, 20, and 28 m, and so on. The path length is adjusted by changing the inclination of the field mirrors at the back end of the cell so that the desired number of passes is achieved and the exiting beam passes through the exit port and onto the detector. Three capacitance pressure gauges are located on a port at the center of the cell with full-scale pressure ranges of 10, 100, and 1000 Torr (760 Torr = 1 atm = 1.01325×10^5 Pa) and accuracies better than 1% of the full-scale reading. The cell can be pressurized up to 12 atm. For these higher pressures, a Heise pressure gauge was used. The cell can be cooled to ~230 K with an accuracy of ±0.5 K over the entire cell volume by circulating methanol cooled with liquid nitrogen through a coil of copper wrapped around the cell and end plates. A feedback control system using a thermocouple mounted in the methanol stream just outside the cell was used to regulate the coolant flow. The temperature of the cell was monitored with three thermocouples mounted on the Invar optical frame in the cell. At thermal equilibrium, these agreed to better than ±0.5 K. Appendix A contains details on the optical design of the long-path cell.

The basic data-collection procedure was to first evacuate the cell and record a background spectrum. The desired amount of water vapor was then added and a pure spectrum recorded. The relative humidity in the cell was kept under ~75% to avoid any possible condensation on surfaces within the cell. Then the broadening gas was added and allowed to stabilize, and another spectrum was recorded. This last step was repeated for several broadening pressures. After spectra were recorded over the desired pressure range, the cell was evacuated and another background run was recorded. A typical set of spectra consists of one pure spectrum and 3 or 4 foreign-broadened spectra with roughly the same water vapor amount. Several sets of these spectra were recorded with variable H_2O partial pressures and path lengths. We initially filled the cell with nitrogen for the background scans but found inconsequential differences between these scans and empty cell scans, so we subsequently just used empty cell scans for the background runs. For the nitrogen-broadened spectra, Scott Ultra Zero Ambient Monitoring Zero grade nitrogen was used. We found that it contained no detectable amounts of CO gas and approximately 2 parts in 10^6 of CO_2, whose bands fortunately do not fall in the spectral region studied in this research.

Most spectra were recorded at an unapodized resolution of 0.040 cm^{-1}. This resolution permits sufficient resolution of important spectral features while limiting the data-collection time and minimizing any long-term drifts in the spectrometer, the detector, and the conditions within the cell. Average run times ranging from 45 min (12-m path length) to over 3 h (84-m path length) were required to achieve adequate signal-to-noise ratios. An added benefit of our relatively low spectral resolution was the ability of the BOMEM processing unit to cover a large enough wave-number range (1150–2250 cm^{-1}) that near 100% transmission baselines could be recorded on both sides of the ν_2 band. As a way to reduce the time for recording a set of spectra further and to minimize any further contributions to noise, the background scans with the cell evacuated were recorded at a resolution of 0.50 cm^{-1}. These were then linearly interpolated in wave number to match the sample runs' resolution with no observable loss in accuracy. Table 1 shows a summary of the parameters for all the data collected, although in this paper we present only the research on the room-temperature self- and N_2-broadened spectra at pressures of 800 Torr and below.

Figure 1 shows an example spectrum in the 1600 cm^{-1} region and calculations using CKDv0, CKDv2.1, and our derived continuum. Note that this region contains the largest differences between the experiment and the CKD models. The spectra show some residual fringes in some spectral regions. This is unimportant for the results presented here because we can easily smooth over these fringes in our relatively wide microwindows.

3. Data Reduction

We use the H_2O continuum definition proposed by Clough *et al.*[7] to report our results. Clough's model is widely used in atmospheric spectroscopy and radiative transfer, particularly in line-by-line codes. Clough defines the local absorption for a single transition as a Lorentz line shape out to ±25 cm^{-1} from the line center, minus the Lorentz value at 25 cm^{-1}. The continuum is then simply defined to be any observed absorption after the removal of the local component. The continuum therefore includes far-wing absorption (beyond 25 cm^{-1} from line center), absorption caused by any near-wing (within 25 cm^{-1}) non-Lorentzian behavior, and the Lorentzian value at 25 cm^{-1} within ±25 cm^{-1} of the line center (this is often called the basement term). The basement term is a relatively minor part of the continuum and is introduced to ensure a smooth continuum for computational reasons. Because the continuum is due to line

Table 1. Summary of the Experimental Parameters for Measured Spectra[a]

Resolution (cm^{-1})	Range (cm^{-1})	P_{H_2O} (Torr)	P_{total} (Torr)	Broadener	T (K)	L (m)
0.04	1050–2250	3, 5, 10, 15	100, 400, 800	Self, N_2	296	84
2.00	1050–7000	3, 5, 10, 15	100, 400, 800	Self, N_2	296	84
0.04	1050–2250	3, 5, 10, 15	100, 400, 800	Self, N_2	260	84
2.00	1050–7000	5	1, 3, 5, 7, 9[b]	Self, N_2	296	84
0.04	1050–2250	3, 5, 10, 15	100, 400, 800	Self, O_2	296	84
0.04	1050–2250	3, 5, 10, 15	100, 400, 800	Self, N_2	296	44
0.04	1050–2250	3, 5, 10, 15	100, 400, 800	Self, N_2	296	12
0.04	1050–2250	5	1, 3, 5, 7, 9[b]	Self, N_2	296	12
0.01	1050–2250	0.03, 7	100, 400, 800	O_2, N_2	296	12
0.04	1050–2250	3, 5, 10, 15	100, 400, 800	Self, N_2	260	12

[a]Temperatures and pressures are approximate (760 Torr = 1 atm = 1.01325×10^5 Pa).
[b]These measurements are in units of atmosphere.

wings, the total continuum absorption coefficient for all lines is formulated as[7]

$$k_{con}(\nu) = P_{H_2O} L \rho_0 \left(\frac{273.15}{T}\right) \nu \tanh\left(\frac{\beta\nu}{2}\right)\left(\frac{296}{T}\right) \times [P_{H_2O} C_s^{\,0}(\nu, T) + P_{N_2} C_f^{\,0}(\nu, T)], \quad (1)$$

where $C_s^{\,0}$ and $C_f^{\,0}$ are the self- and foreign-broadened continuum coefficients at 296 K and 1 atm, ρ_0 is the absorber number density per atmosphere at 273.15 K, and $\beta = hc/kT$. In window regions, $C_s^{\,0}$ and $C_f^{\,0}$ vary smoothly with wave number because there are relatively few strong local absorption lines. Within strong absorption bands, however, the continuum may be influenced more by high-frequency near-wing non-Lorentzian behavior, and these continuum coefficients may not vary as smoothly with wave number. Figure 2 shows the individual contributions of the far-wing, near-wing, and basement components to the total continuum in the ν_2 region based on the use of CKDv0. Although the continuum is dominated by far-wing effects in the wings of the ν_2 band, the near-wing contributions dominate the continuum at the peaks of the P and R branches.

To determine the experimental continuum from the raw data, we first ratioed the absorption scans to the average of the background scans. The 100% transmission level was fine tuned by checking the transmission in two regions of very low absorption on each side of the ν_2 band. We observed a small discontinuity in the 100% transmission levels near 1700 cm^{-1} in many runs that could range from near zero to several percent. Consequently, between 1700 cm^{-1} and higher frequencies, we multiplied the transmission by a scalar to force agreement with the calculated transmission in a very transparent window in the high-wave-number wing of the band. A similar scalar adjustment was applied between the low-wave-number side of our spectra and 1700 cm^{-1}, but it was now based on the difference between observed and computed transmissions in a window area in the low-wave-number side of the band. The calculated transmission was based on the use of CKDv2.1. Modifications to the 100% transmission were very small, typically of the order of 0.005 in transmission. For this reason, we do not believe that various phenomena, such as condensation of water vapor onto the cell window and mirror surfaces, which would

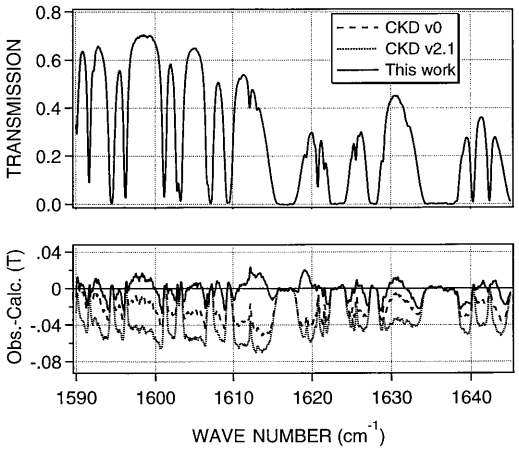

Fig. 1. Measured spectrum and calculations for 14.5-Torr H_2O, 804-Torr N_2, 296.1 K, 12.05-m path length.

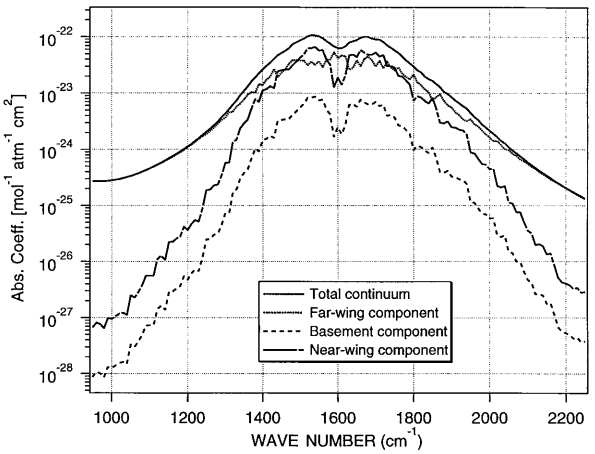

Fig. 2. Individual contributions of the far-wing (beyond 25 cm^{-1}), near-wing (within 25 cm^{-1}), and basement components to the total continuum absorption based on the use of CKDv0 (see Section 3 and Subsection 4.A).

lead to erroneous results, were present during the data collection, or at least did not produce a detectable effect. In addition, no unexpected changes in the throughput of the cell with the addition of water vapor (except for the obvious absorption caused by gaseous water vapor) or with increased path length was observed.

We determined the continuum in the microwindows by utilizing the pressure dependencies of Eq. (1). This approach decreases sensitivity to uncertainties in the 100% transmission baseline, because the fitted continuum coefficients only depend on the slope of k_{con} with pressure and not on the absolute value of the experimental continuum. For pure H_2O spectra, C_s^0 is proportional to the slope of the observed continuum absorption coefficient versus $P_{H_2O}{}^2$. Similarly, for N_2-broadened spectra with the same H_2O partial pressure, C_f^0 is proportional to the slope of the observed continuum absorption coefficient versus P_{N_2}. Our reported results come from least-squares fits for these slopes.

For a single spectrum, in any given window region, the uncertainty in the continuum absorption coefficient is mainly due to uncertainties in (a) the actual H_2O pressure, (b) the 100% transmission baseline, and (c) the line parameters used to subtract off the local absorption contribution.

A. H_2O Partial Pressures

In regions of good optical depth, the main source of experimental error for this research is the uncertainty in the amount of H_2O in the cell after the addition of a broadening gas. For pure water vapor samples, the water vapor pressure can be measured directly with the capacitance pressure gauges attached to the cell. However, when a broadening gas is added, the water vapor has a tendency to adsorb onto the cell walls and other surfaces.[13] Because our spectral resolution is sufficient to resolve well-isolated N_2-broadened H_2O lines, we monitored the H_2O partial pressure by using the observed spectra. The H_2O partial pressure was determined by fitting isolated lines in the band wings (1090–1375 cm^{-1} and 1800–2240 cm^{-1}) to Lorentzian profiles by using the following expression:

$$k(\nu) = P_{H_2O} L \frac{S}{\pi} \frac{\gamma_{\mathrm{obs}}}{[\gamma_{\mathrm{obs}}{}^2 + (\nu - \nu_0 - \delta\nu)^2]}, \qquad (2)$$

where the water vapor pressure, P_{H_2O}, the observed half-width, γ_{obs}, and a possible line shift, $\delta\nu$, were allowed to vary. Here S is the line strength, ν_0 is the line center, and ν is the wave number. Allowing the linewidth to float effectively decouples the fit from uncertainties in the width and residual instrument broadening. Note that the width term does not explicitly include P_{H_2O}, effectively decoupling the dependency of the fitted H_2O partial pressure from the observed linewidth. The quality of these fits was very high, with residuals caused only by noise in the data. We averaged the H_2O partial pressures returned by fits to 30–40 spectral lines on each side of the band. The statistical error in these averages is 3–4%. This error is probably a combination of uncertainties in the high-resolution transmission molecular absorption (HITRAN) line strengths and our measurement errors.

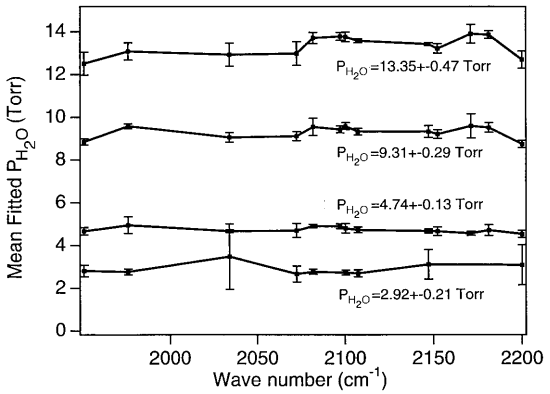

Fig. 3. Water vapor partial pressures determined for four sets of N_2-broadened spectra in the high-wave-number band wing. Error bars are determined by averaging over results obtained from spectra at various N_2 pressures.

Figure 3 shows the fitted water vapor pressures for several lines in the high wave-number wing for four sets of N_2-broadened spectra. It is likely that the relative strengths of isolated lines in the HITRAN database are quite accurate,[25] so it is not surprising that our statistical error in the H_2O partial pressure is so low. Systematic errors in the line strengths will of course affect our determination of the H_2O partial pressure. However, because we use a strength–pressure product that is derived from the spectra to compute the local absorption, systematic errors in the line strengths will partially cancel in our continuum determinations.

Our derived H_2O partial pressures indicate that roughly 5% of the water vapor was adsorbed onto the cell walls with the addition of the first ~100 Torr of N_2 (or O_2). However, we found no evidence that the H_2O partial pressure changed thereafter, allowing us to use an average H_2O partial pressure derived from spectra at all pressures in each data set. This is illustrated in Fig. 4 for a line at ~2081 cm^{-1}, where the slope of the fitted water vapor pressure versus increasing total cell pressure is essentially zero.

B. Baseline Errors

The sensitivity of the derived continuum to uncertainties in the 100% transmission baseline was determined as follows. Instead of deriving the continuum from the slope of Eq. (1), we can instead calculate it directly from this relation by using a single spectrum. For the N_2 continuum this does require that one first measures the self-continuum contribution so it can be subtracted from k_{con}. This method is prone to large errors because it is very sensitive to uncertainties in the 100% transmission baseline, especially in regions of low absorption. By comparing results obtained with this error-prone

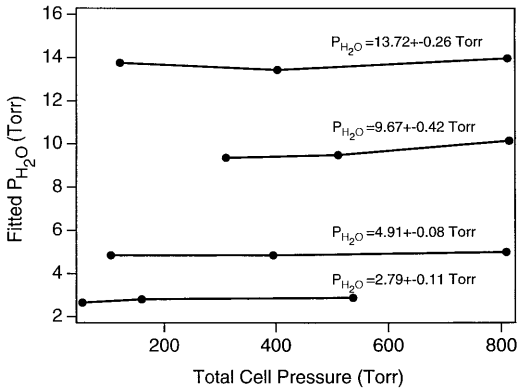

Fig. 4. Water vapor partial pressures determined for spectra at various N_2 pressures from a line at ~2081.0 cm^{-1}.

method with those obtained with the slope method, we can quantify the uncertainty in the measured transmission baselines. The differences in these two measurements indicate that we have maximum baseline errors of roughly ~0.005 in transmission. We used this baseline error to determine errors in the continuum derived with the slope method. The impact of this error will vary strongly with spectral region. In regions of strong absorption, the resulting errors in the retrieved continuum coefficients caused by baseline errors are negligible compared with the uncertainty in the H_2O partial pressure. However, in regions of little absorption, the baseline error is potentially the main source of error in the coefficients. For example, at ~1350 cm^{-1}, a 0.005 baseline error in transmission translates into an error of approximately 30–40% in C_f^0 for our optical depths.

We propagated a baseline error of 0.005 in transmission into the uncertainty of the continuum coefficients reported here. This appears to be a good estimate for the low-wave-number band wing, where the spectra are dominated by noise. However, in the high-wave-number wing, the signal-to-noise ratio is much greater and it appears that we may have overestimated the baseline error in this region, where we report large uncertainties despite the excellent agreement with Burch's measurements (see Section 4).

C. Local Line Parameters

Line positions and strengths used to calculate the local line absorption were taken from the 1992 HITRAN database,[25] which consists primarily of measurements by Toth[26] for the ν_2 band of $H_2^{16}O$. Self-broadened widths were also provided by Toth.[27] For the strong lines at the center of the $H_2^{16}O$ ν_2 fundamental, the nitrogen-broadened half-width measurements of Remedios[28] were used. His corresponding air-broadened widths are currently on the HITRAN database. Toth's measured values of nitrogen-broadened half-widths[27] were used for the $H_2^{18}O$ and $H_2^{17}O$ lines. For all remaining lines, the HITRAN air-broadened values[25] were used, divided by a factor of 0.9 to convert them to nitrogen broadening. This is valid for most remaining lines because the original calculations by Gamache and Davies[29] were done for nitrogen broadening and multiplied by 0.9 to convert to broadening by air.

The sensitivity of the retrieved continuum coefficients to inaccuracies in these line parameters was tested by producing synthetic spectra, from which we derived the continuum by using artificially perturbed line parameters. The line parameters were perturbed by nominal accuracies of the linewidths (approximately ±10%) and line strengths (approximately ±5%). These errors may be somewhat conservative, because the strengths of many of the strongest lines have quoted accuracies of 2% and 3%. Furthermore, Toth's nitrogen-broadened widths for $H_2^{18}O$ have quoted uncertainties of 3–5%. Independent nitrogen-broadened half-width measurements have also been performed by using the spectra we collected at a resolution of 0.011 cm^{-1}, and good agreement is found with the values of Remedios for the $H_2^{16}O$ lines. For lines that have optimum measurement conditions, we find agreement to within 2–3%. The sensitivity analysis resulted in continuum errors in the microwindows ranging from approximately 1–2% to greater than 10%, depending on the width of the window and its sensitivity to the local absorption coefficient. As expected, the best windows are located at the very center and in the wings of the band. The windows most sensitive to line parameter errors are located at the peaks of the P and R branches.

D. Total Error Budget

We used a simple propagation of errors to combine the above sources of errors in determining uncertainties of 1 standard deviation in the reported continuum coefficients. These errors were calculated separately for each continuum coefficient we report. For example, for a series of pure spectra with various H_2O partial pressures, the continuum absorption coefficient would be plotted versus $P_{H_2O}{}^2$, with each point having its own uncertainty dependent on (a) the baseline errors for the spectrum used to determine k_{con} for that point, (b) the uncertainty in the local absorption coefficient subtracted from that spectrum, and (c) the uncertainty in P_{H_2O}. A weighted linear fit of this curve gives $C_s{}^0$ and its statistical uncertainty, which is combined with the uncertainty in $C_s{}^0$ from the propagation of errors. This results in one retrieved value of the continuum coefficient and its uncertainty. We then combine values for the same wave-number region obtained from spectra taken at different path lengths by using a weighted mean, where the final error is a combination of the standard deviation of the mean and the propagation of errors' uncertainty. The pure spectra were grouped and analyzed individually according to path lengths of 12, 44 and 84 m. A final value for $C_s{}^0$ was derived from a weighted sum of these three measurements. For the N_2-broadened spectra, the spectra were grouped according to different path lengths and H_2O pressures, resulting in 12 groups that were then com-

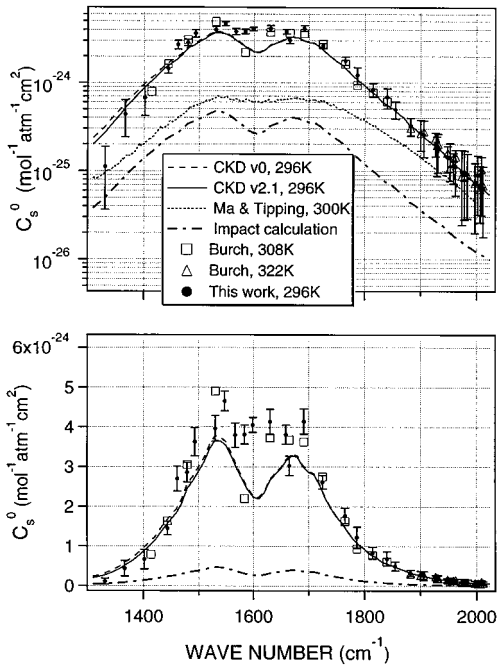

Fig. 5. Self-broadened continuum coefficients from this research, Burch, CKD models, Ma and Tipping, and impact theory.

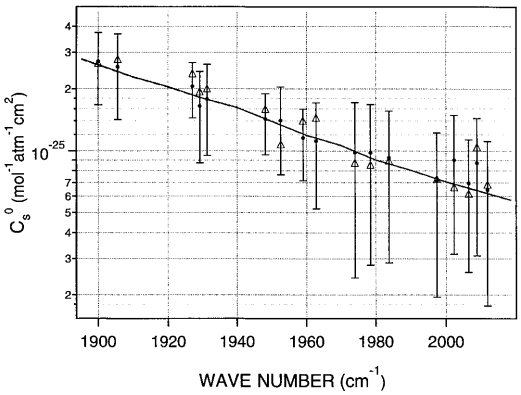

Fig. 6. Expanded portion of Fig. 5.

bined into one final value of C_f^0 and its associated uncertainty.

4. Discussion of Results

A. Self-Broadened Continuum

Self-broadened continuum results are plotted in Fig. 5 in a semilog (top panel) and linear (bottom panel) format, along with the measurements of Burch[14] and Clough's CKDv0 and CKDv2.1 models.[8] Burch's measurements have been modified to be consistent with the local line-shape definition used here and were provided by Clough. The theoretical calculations of Tipping and Ma[5] are also shown, although it should be emphasized that their published results are not directly applicable to the in-band continuum for several reasons. Continuum measurements are also included for a number of additional microwindows that Burch did not report. Our uncertainties are quite small between 1450 and 1900 cm^{-1}, i.e., of the order of 10%. In the edges of the band, these accuracies increase because of increased noise, especially at the lower wave numbers, and because of a lack of optical depth. A calculation using the impact approximation (Van Vleck–Huber) in Fig. 5 clearly shows that the absorption is super-Lorentzian within the band.

The most obvious difference between our results and those of Burch is at 1584.0 cm^{-1}, where Burch's continuum is almost half of our result. Otherwise, we find general agreement with Burch. Indeed many of his measurements fall within the error bars of our results. In the high-wave-number wing, there is good agreement with Burch's measurements at 322 K and with Clough's models. A comparison of our 296-K data to Burch's 322-K measurements shows no observable temperature dependence of C_s^0 in this region at the level of accuracy of the data. A blowup of the high-wave-number continuum in Fig. 6 shows better agreement of our results with Clough's CKD models than with Burch's points.

These results suggest that the dip at the band center is not as drastic as that seen by Burch. Burch's only point that follows this dip in the continuum is the one at 1584 cm^{-1}, where our measurement is almost twice as large. We cannot find any reason why our reported uncertainty in this region should be any larger and can only conclude that the difference is due to an error in Burch's measurement. Note that we also see rather large differences between our results and Burch's at the band center for the N_2-broadened continuum as well. Also note that in Fig. 2, the dip in the total continuum is caused by the near-wing line-shape behavior (within 25 cm^{-1} of the line center), at least according to Clough's definition of the continuum.

As we mentioned above, Ma and Tipping's theoretical calculations are not directly applicable to the in-band continuum. Their theory is by nature a far-wing theory and is least accurate close to line centers. Furthermore, they used a 25-cm^{-1} cutoff, so that contributions from lines within $\pm$25 cm^{-1} of the line center were not adequately represented in these calculations. We have added the basement terms to their calculations for consistency. In a very rough sense, Fig. 2 shows that lines within 25 cm^{-1} contribute of the order of half the observed continuum, so it is not surprising that Ma and Tipping's results are so much smaller than our measurements. Their calculations do agree better with the experiment in the wings of the band where the continuum is due almost entirely to the far wings of lines. Our in-band measurements should help guide future theoretical research on the near-wing line shape.

B. N_2-Broadened Continuum

N_2-broadened continuum results are plotted in Fig. 7 in a semilog (top panel) and linear (bottom panel) format, along with the measurements of Burch[14] and Clough's CKDv0 and CKDv2.1 models.[8] The theo-

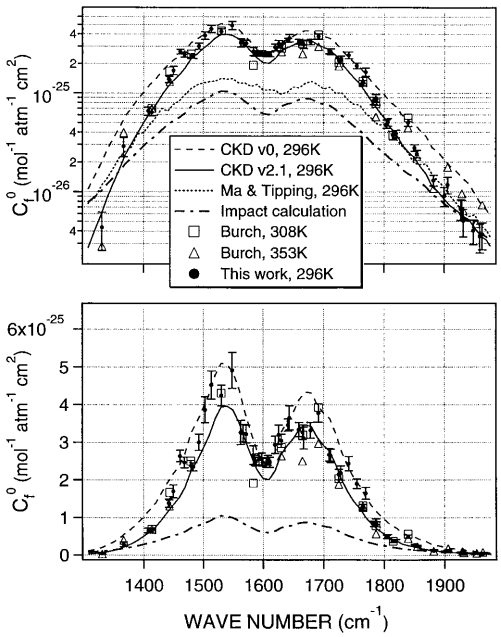

Fig. 7. N_2-broadened continuum coefficients from this research, Burch, CKD models, Ma and Tipping, and impact theory.

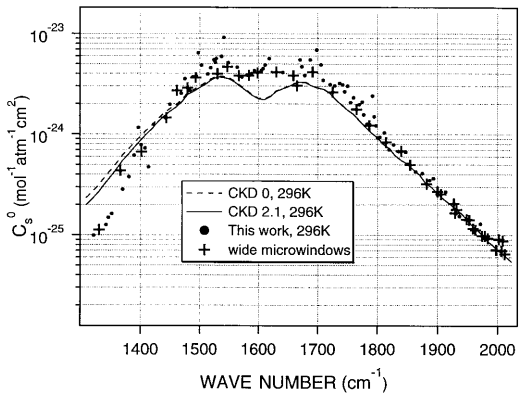

Fig. 8. Self-broadened continuum coefficients from this research reported for a larger number of microwindows (see Subsection 4.C).

retical calculations of Ma and Tipping are again included; keep in mind, however, that their calculations are really only applicable to the wings of the band, as we discussed above. Impact calculations (Van Vleck–Huber) are also shown. These figures include measurements of C_f^0 in a few additional microwindows that Burch did not report. Our best results are located between 1450 and 1900 cm^{-1}, where the uncertainties are of the order of 10%. Just as for the self-broadened data, the reported uncertainties in the band wings are dominated by the estimated 0.5% uncertainty in the 100% transmission level.

As with self-broadening, the largest discrepancy between these measurements and Burch's is the point at 1584 cm^{-1}, near the center of the band, where Burch's value is approximately 30% smaller than ours. From 1500 to 1700 cm^{-1} the N_2-broadened continuum values are all lower than Burch's. In this same region our results follow Clough's CKDv0 curve much better than that of CKDv2.1. Above 1700 cm^{-1} both our data and Burch's jump between Clough's two models. Our results are in rough agreement with those of Burch except past 1950 cm^{-1}, where our error bars start to get large. In this region, however, our results are in good agreement with the measurements of Thériault.[17] Above 1850 cm^{-1} all of Burch's points are for 353 K, while our data are at 296 K, so some disagreement is not unexpected. The overall agreement of our data with that of Burch above 1700 cm^{-1} proves that the continuum is indeed bumpy and that a smooth continuum such as Clough's present models cannot adequately reproduce the data.

Below 1500 cm^{-1} there is rough agreement with Burch, except for the lowest wave-number point at 1333.1 cm^{-1}, where our error bars become large. Although there are fewer microwindows on this side of the band, the measured continuum still bounces to some degree between Clough's CKDv0 and CKDv2.1. Below 1450 cm^{-1} our data seem to favor CKDv2.1. This region has fewer wide microwindows, so we did not add many more points over what Burch used.

On the low-wave-number side of the band, our measurements are in general agreement with Thériault's results[17] for measurements at the exact centers of the microwindows. From ~1320 to 1360 cm^{-1}, our values for C_f^0 agree with those of Thériault within experimental error. However, at Thériault's highest wave number in this region (~1381 cm^{-1}) our value is twice as large as Thériault's, with Clough's CKDv2.1 falling almost directly in between the two measurements. On the high-wave-number side of the band, our results are in relatively good agreement with Burch's measurements and with CKDv2.1, all of which are consistently larger than Thériault's results.

C. Continuum in Narrower Microwindows

Our H_2O spectra contain a large number of microwindows that are not as wide as those used by Burch but are still relatively free of strong local absorption. In Figs. 8 and 9 the measured values for C_s^0 and C_f^0 for a number of additional microwindows are shown. We loosely define these windows as spectral regions that contain a local transmission maximum that is at least 0.5 cm^{-1} wide and is not too close to a very strong line. Because the ultimate goal is to reproduce the observed spectra, we eventually hope to develop a model that will work on any wave-number grid. An examination of the continuum in these smaller microwindows by using Clough's existing continuum definition is a natural first step.

The self-broadened results shown in Fig. 8 suggest that the continuum becomes quite bumpy with wave number between the strong lines of the band. Most of the new points in this graph are larger than those in the original microwindows, indicating that near-wing super-Lorentzian behavior by the local lines is playing an important role in the observed absorption coefficients, although these regions are also more sensitive to inaccurate line parameters. Note that our

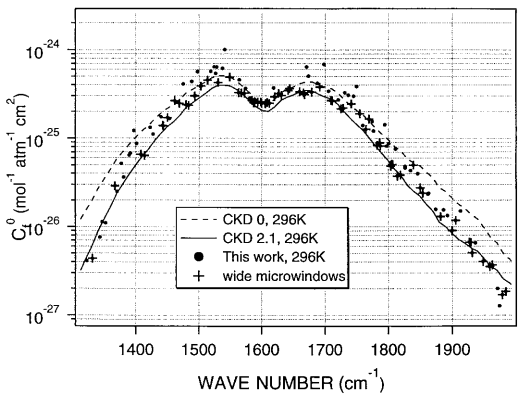

Fig. 9. N_2-broadened continuum coefficients from this research reported for a larger number of microwindows (see Subsection 4.C).

continuum is fairly smooth near the band center and in the band wings where there is an absence of strong lines.

The N_2-broadened continuum shown in Fig. 9 is quite a bit bumpier than the self-continuum. Again, most of the added points have a larger continuum than those in the original larger microwindows. When compared with the self-broadened results, the more extreme bumpiness in these results may indicate that local line super-Lorentzian behavior is even larger for N_2 broadening than for self-broadening. This is consistent with Ma and Tipping's research,[30,31] which states that the N_2-broadened line shape is more super-Lorentzian close to the line centers than the self-broadened line shape. This effect could, however, be an artifact of the data analysis because the nitrogen-broadened spectra have more optical depth closer to the line centers and are thus more sensitive to linewidth errors.

5. Conclusions

Experimental measurements of the ν_2 water vapor continuum coefficients have been determined and compared with the previous results of Burch *et al.* In regions that are least sensitive to local line absorption, these coefficients are in general agreement with the earlier measurements as well as with the CKD models. However, our results show that accurate modeling of the continuum within the band will require a much more complex model; possibly super-Lorentzian local line shapes will be required. In fact, it may be necessary to redefine the meaning of the local component of the continuum and use a non-Lorentzian local line shape.

We plan to extend our analysis to a denser wavenumber scale in spectral regions closer to strong absorption lines. This will require great care because of the difficulty in differentiating between the effects of incorrect spectral line shapes, line strengths, and linewidths. Preliminary results indicate that in regions of strong local absorption, the continuum is dominated by near-line super-Lorentzian line-shape behavior and cannot be modeled smoothly as a function of wave number.

Appendix A: Multiple Reflection Absorption Cell

The modified White-type multiple reflection absorption cell was designed and constructed to interface to the NIST BOMEM Fourier transform spectrometer (FTS). The three mirrors with a radius of curvature of 2 m are of Zerodur and are mounted on a frame connected rigidly only to the front end of the enclosing tank. The separation of the mirrors is maintained by four rods of super-Invar for temperature independence of the optical system. The rest of the system was fabricated of stainless steel and is sealed with fluorosilicone O rings.

The NIST BOMEM DA3.002 FTS has for the largest aperture a diameter of 1 cm, a beam-splitter radius of 3.81 cm, and a focal length of 45.72 cm. Thus the square root of the étendue divided by π is 1/24 cm for this aperture. The evacuated transfer optics puts an image of the FTS magnified by a factor of 3.175, radius $R_a = 1.587$ cm, at the entrance of the White cell, and simultaneously, without use of a field lens, puts an image of the beam splitter of radius 5.2493 cm on the top back mirror of the White cell, thus matching the étendue of the White cell to that of the FTS.

The height of the front mirror is large enough to permit 22 transits for a 44-m path length with this maximum image size. For other FTS apertures, 7 mm permits 30 transits, 5 mm permits 42 transits, and 3.5 mm permits 58 transits. Some adjustment of the transfer optics is required when the aperture size is changed, because the bottom of the circular input image must be tangent to the upper edge of the front mirror for close packing of the images in columns.

The optical system of the modified White cell is shown in Fig. 10. In this configuration the entrance beam comes to the top back mirror, M1, and the exit beam leaves from the same mirror. This permits separation of the two columns of images on the front spherical mirror. It is possible to almost eliminate astigmatism for a single point in the image by a choice of the ratio of W to H. (See Fig. 10). When this is done, it is found by ray tracing that the astigmatism around the outside circumference of the whole output image is considerably reduced compared with a White cell where W is a minimum, i.e., just one image diameter.

For each object–image pair on the front mirror there is an off-axis angle associated with the back mirror that forms the image, and this has both vertical and horizontal components with respect to a spaced fixed, say, horizontal plane. The horizontal component is constant, but the vertical components vary. Hannan's[32] treatment has been used with small-angle approximations to derive a simple analytical expression for the ratio of W to H. An independent derivation leads to the same result, but this is only good to a few percent. The simple analytical results given below have been refined by ray tracing. The condition for vanishing of astigmatism at the center of the output image is

$$W/H = [(N + 2)/3(N - 2)]^{1/2}, \quad (3)$$

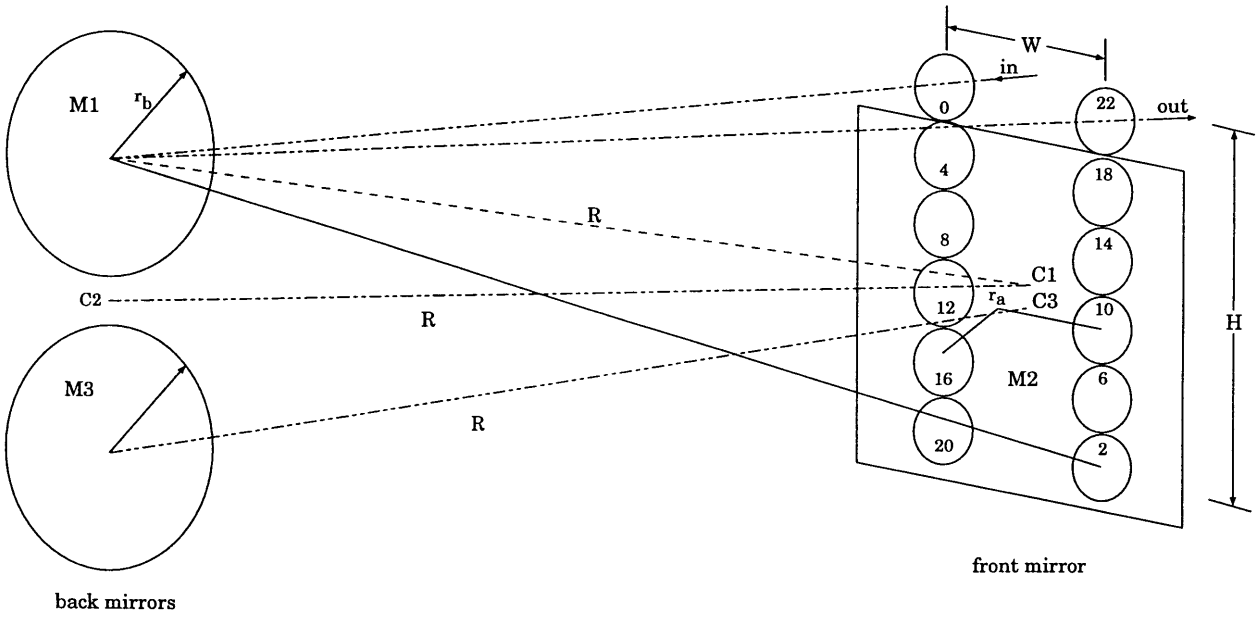

Fig. 10. Modified White cell design: C1, C2, and C3 are centers of curvature of mirrors M1, M2, and M3, respectively.

where N is the total number of transits. At approximately this value of W/H the astigmatism goes through an inversion, having a different sign for higher values of W/H. Actually it is more useful to balance the astigmatism for the inside and outside of the output image, and for this the condition at the center of the image is

$$W = r_a[(N^2 - 52)/48]^{1/2}, \tag{4}$$

where r_a is the ideal image radius. Because $H = r_a(N - 2)/4$,

$$W/H = [(N^2 - 52)/3(N - 2)^2]^{1/2}. \tag{5}$$

With astigmatism balanced but of opposite sign at the inside and outside of the image, it is found that this remaining image broadening is lower than that with $W = 2r_a$ by a factor that increases with the number of passes, being approximately five for 82 transits. For a first approximation, to obtain minimum astigmatism for less than the maximum number of transits, one should adjust the first back mirror so the first image on the front mirror is at the same position as for maximum transits, and then adjust the other back mirror for the desired number of transits. There is a variation of this optical configuration in which the two back mirrors are rotated together, but one can only minimize astigmatism for some fixed number of transits when the back mirrors are thus constrained.

This research was supported by NASA under grant NAG 05-5-28045. We thank R. A. Toth for the use of his line parameters provided to us before publication. W. J. Lafferty acknowledges support from the Upper Atmosphere Research Program of NASA. The authors thank S. E. Hannon, M. E. Thomas, G. Birnbaum, R. R. Gamache, S. A. Clough, R. H. Tipping, and Q. Ma for their help and comments.

References and Notes

1. W. B. Grant, "Water vapor absorption coefficients in the 8–13 μm spectral region: a critical review," Appl. Opt. **29,** 451–462 (1990).
2. M. E. Thomas, "Infrared and millimeter wavelength continuum absorption in the atmospheric windows: measurements and models," Infrared Phys. **30,** 161–174 (1990).
3. AIRS Project Office, "Atmospheric Infrared Sounder: science and measurement requirements," Tech. Rep. D6665 Rev. 1 (Jet Propulsion Laboratory, Pasadena, Calif., 1991).
4. H. H. Aumann and R. J. Pagano, "Atmospheric Infrared Sounder on the Earth Observing System," Opt. Eng. **33,** 776–784 (1994).
5. R. H. Tipping and Q. Ma, "Theory of the water vapor continuum and validations," Atmos. Res. **36,** 69–94 (1995), and references therein.
6. S. A. Clough, F. X. Kneizys, R. Davies, R. Gamache, and R. Tipping, "Theoretical lineshape for the H_2O vapor: application to the continuum," in *Atmospheric Water Vapor*, A. Deepak, T. D. Wilkerson, and L. H. Ruhnke, eds. (Academic, New York, 1980), pp. 25–46.
7. S. A. Clough, F. X. Kneizys, and R. W. Davies, "Line shape and the water vapor continuum," Atmos. Res. **23,** 229–241 (1989).
8. S. A. Clough, in "The water vapor continuum and its role in remote sensing," in *Optical Remote Sensing of the Atmosphere*, Vol. 2 of 1995 OSA Technical Digest Series (Optical Society of America, Washington, D.C., 1995), pp. 76–78.
9. P. W. Rosenkranz, "Pressure broadening of rotational bands. I. A statistical theory," J. Chem. Phys. **83,** 6139–6144 (1985).
10. P. W. Rosenkranz, "Pressure broadening of rotational bands. II. Water vapor from 300 to 1100 cm^{-1}," J. Chem. Phys. **87,** 163–170 (1987).
11. Q. Ma and R. H. Tipping, "A near-wing correction to the quasistatic far-wing line shape theory," J. Chem. Phys. **100,** 2537–2546 (1994).
12. Q. Ma and R. H. Tipping, "An improved quasistatic line-shape theory: the effects of molecular motion on the line wings," J. Chem. Phys. **100,** 5567–5579 (1994).

13. D. E. Burch, D. A. Gryvnak, and R. R. Patty, "Absorption of infrared radiation by CO_2 and H_2O. Experimental techniques," J. Opt. Soc. Am. B **57,** 885–895 (1967).
14. D. E. Burch, "Continuum absorption by H_2O," Ford Aerontronic Rep. AFGL-TR-81-0300 (U.S. Air Force Geophysics Laboratory, Hanscom Air Force Base, Mass., 1981).
15. D. E. Burch and R. L. Alt, "Continuum absorption by H_2O in the 700–1200 cm^{-1} and 2400–2800 cm^{-1} windows," Rep. AFGL-TR-84-0128 (U.S. Air Force Geophysics Laboratory, Hanscom Air Force Base, Mass., 1984).
16. D. E. Burch, "Absorption by H_2O in narrow windows between 3000 and 4200 cm^{-1}," Rep. AFGL-TR-85-0036 (U.S. Air Force Geophysics Laboratory, Hanscom Air Force Base, Mass., 1985).
17. J.-M. Thériault, P. L. Roney, D. St.-Germain, H. E. Revercomb, R. O. Knuteson, and W. L. Smith, "Analysis of the FASCODE model and its H_2O continuum based on long path atmospheric transmission measurements in the 4.5–11.5 μm region," Appl. Opt. **33,** 323–333 (1994).
18. W. L. Smith, H. E. Revercomb, H. B. Howell, H.-L. Huang, R. O. Knuteson, D. D. LaPorte, E. W. Koenig, S. Silverman, L. A. Sromovsky, and H. M. Woolf, "GHIS—the GOES high-resolution interferometer sounder," J. Appl. Meteorol. **29,** 1189–1204 (1990).
19. S. A. Clough, R. D. Worsham, W. L. Smith, H. E. Revercomb, R. O. Knuteson, G. P. Anderson, M. L. Hoke, and F. X. Kneizys, "Validation of FASCODE calculations with HIS spectral radiance measurements," in *Proceedings of the International Radiation Symposium '88*, J. Lenoble and J.-F. Geleyn, eds. (Deepak, Hampton, Va., 1989), pp. 376–379.
20. H. E. Revercomb, R. O. Knuteson, W. L. Smith, H. M. Woolf, and H. B. Howell, "Spectroscopic inference from HIS measurements of atmospheric thermal emission," in *Optical Remote Sensing of the Atmosphere*, Vol. 4 of 1990 OSA Technical Digest Series (Optical Society of America, Washington, D.C., 1990), pp. 590–595.
21. H. E. Revercomb, W. L. Smith, R. O. Knuteson, H. M. Woolf, and H. B. Howell, "Comparison of FASCODE spectra with HIS observations," in *Annual Review Conference on Atmospheric Transmission Models* (U.S. Air Force Geophysics Laboratory, Hanscom Air Force Base, Mass., 1989).
22. L. L. Strow, D. C. Tobin, and S. E. Hannon, Department of Physics, University of Maryland Baltimore County, Baltimore, Md. 21228 (personal communication, CAMEX/HIS calculations with CKDv2.1), 1995.
23. The mention of brand names in this paper is for information purposes only and does not constitute an endorsement of the product by the authors or their institutions.
24. W. B. Olson, "Method for first-order design of a transfer optics system to throughput match a Fourier transform spectrometer to a sample cell without use of a field lens at the cell input," Appl. Opt. **26,** 2441–2445 (1987).
25. L. S. Rothman, R. R. Gamache, R. H. Tipping, C. P. Rinsland, M. A. H. Smith, D. C. Benner, V. Malathy Devi, J.-M. Flaud, C. Camy-Peyret, A. Perrin, A. Goldman, S. T. Massie, L. R. Brown, and R. A. Toth, "The HITRAN molecular database: editions of 1991 and 1992," J. Quant. Spectrosc. Radiat. Transfer **48,** 469–507 (1992).
26. R. A. Toth, "ν_2 band of $H_2^{16}O$: line strengths and transition frequencies," J. Opt. Soc. Am. B **8,** 2236–2255 (1991).
27. R. A. Toth, Jet Propulsion Laboratory, Pasadena, Calif. 91109 (personal communication, 1994).
28. J. J. Remedios, Ph.D. dissertation (Oxford University, New York, 1990).
29. R. R. Gamache and R. W. Davies, "Theoretical calculations of N_2-broadened halfwidths of H_2O using quantum Fourier transform theory," Appl. Opt. **22,** 4013–4019 (1983).
30. Q. Ma and R. H. Tipping, "A far wing line shape theory and its application to the water vibrational bands (II)," J. Chem. Phys. **96,** 8655–8663 (1992).
31. Q. Ma and R. H. Tipping, "A far wing line shape theory and its application to the foreign-broadened water continuum absorption (III)," J. Chem. Phys. **97,** 818–830 (1992).
32. P. Hannan, "White cell design considerations," Opt. Eng. **28,** 1180–1184 (1989).